Research Article

INTERNATIONAL JOURNAL OF ADVANCED ROBOTIC SYSTEMS

International Journal of Advanced Robotic Systems
May-June 2018: 1–10

DOI: 10.1177/1729881418783413
journals.sagepub.com/home/arx
SAGE

An active contour model for brain magnetic resonance image segmentation based on multiple descriptors

Chen Hong[1,2], Yu Xiaosheng[1], Wu Chengdong[1] and Wu Jiahui[1]

Abstract

With the increasing use of surgical robots, robust and accurate segmentation techniques for brain tissue in the brain magnetic resonance image are needed to be embedded in the robot vision module. However, the brain magnetic resonance image segmentation results are often unsatisfactory because of noise and intensity inhomogeneity. To obtain accurate segmentation of brain tissue, one new multiphase active contour model, which is based on multiple descriptors mean, variance, and the local entropy, is proposed in this study. The model can bring about a more full description of local intensity distribution. Also, the entropy is introduced to improve the performance of robustness to noise of the algorithm. The segmentation and bias correction for brain magnetic resonance image can be simultaneously incorporated by introducing the bias factor in the proposed approach. At last, three experiments are carried out to test the performance of the method. The results in the experiments show that method proposed in this study performed better than most current methods in regard to accuracy and robustness. In addition, the bias-corrected images obtained by proposed method have better visual effect.

Keywords

Robot vision, segmentation, brain MR image, active contour model, bias correction

Date received: 23 May 2017; accepted: 23 May 2018

Topic: Vision Systems
Topic Editor: Antonio Fernandez-Caballero
Associate Editor: José Manuel Ferrández Vicente

Introduction

With the development of pattern recognition, artificial intelligence, and image processing technology, various kinds of robotics have been widely used. Robots mainly include the following three kinds: first, industrial robotics applied to manufacturing, logistics, and agriculture. Second, special robotics used in medical and other fields. Third, service robotics applied to customer service, escort, and design. Medical robotics is the robotics that has been applied in many medical fields, such as diagnosis, treatment, rehabilitation, nursing, and functional assistance. Among them, surgical robots are the most widely used and promising. The powerful functions they provide overcome the poor accuracy, long operation time, fatigue, and lack of vision in traditional surgery.

Currently, encephalopathy is one of the serious diseases that threaten people's health. With the development of medical technology and robotics, brain surgery robots have been increasingly used in the planning, navigation, and orientation of cerebral surgery. And the computer vision has been applied in neurosurgery[1,2] and robotic brain

[1] Faculty of Robot Science and Engineering, Northeastern University, Shenyang, China
[2] College of Physics Science & Technology, Anshan Normal University, Anshan, China

Corresponding author:
Chen Hong, Northeastern University, No. 3-11, Wenhua Road, Helping District, Shenyang 110819, People's Republic of China.
Email: chenhongbuty@126.com

surgery.[3–5] Brain surgery robot uses embedded computer vision module to collect brain image data, and then accurately segment, detect, and locate brain tissue. Due to the accurate segmentation algorithm, precise location information of brain tissue can be used during brain surgery. Image segmentation is the foundation of computer vision applications. In the computer vision module of the brain surgery robot, the segmentation effect of the brain image directly determines the positioning accuracy and the success rate of the operation. However, the brain magnetic resonance (MR) image segmentation is difficult because of the complicated brain structure and the inferior quality image. The brain MR image is affected by acquisition sequences and radio frequency coils. So the intensity variation across the image reflects the intensity inhomogeneity. Also, image is usually vulnerable to noise that causes unexpected results. Therefore, more accurate and robust segmentation algorithms for brain image with intensity inhomogeneity and noise are very important and necessary. And the algorithm should meet the following four conditions. The first one refers to the full description of gray value distribution, which can overcome the intensity inhomogeneity and ensure segmentation accuracy. The second one is that it should be robust to serious noise. Third, it can implement the multiphase segmentation. Finally, the bias field can be estimated.

In the past decades, many active contour models (ACMs) that are considered as a well-performed class of segmentation algorithms with promising result have been proposed.[6] For the sake of images with intensity, some ACMs introduce the local grayscale statistics.[7–10] Vese and Chan[7] provided a piecewise model, which can solve the problem in some case. The method is computationally inefficient, which limits its application. Li et al.[8] presented an ACM with local binary fitting (LBF) energy to obtain the correct object boundaries in segmentation images with inhomogeneous intensity. Subsequently, a number of methods were proposed, whose effects were similar to LBF.[11,12] However, the LBF method fails to achieve accurate results sometimes because the local intensity information is only represented by means. It is not enough to describe intensity distribution in a local domain with same mean and different texture. To solve the problem, Wang et al. presented a new ACM based on local Gaussian distribution fitting energy.[9] In the local Gaussian distribution fitting (LGDF) model, the local grayscale statistics are described not only with means but also with variances, which enable LGDF with better robustness on the intensity inhomogeneity. However, the above methods could not work very well for segmenting the brain MR image.

Recently, some novel ACM-based brain MR image segmentation methods have been proposed in literature.[13–21] However, these methods have different drawbacks and cannot provide the desirable results. The method proposed by Akram et al.[13] is not able to carry out the bias field estimation. The methods proposed by Li et al.,[14,15] Gharge and Bhatia,[16] and Konduri and Thirupathaiah[17] cannot accurately describe the local intensity distribution of brain MR image. The methods proposed by Gharge and Bhatia,[16] Konduri and Thirupathaiah,[17] and Zhang[18] cannot be used to implement multiphase segmentation for brain tissue. The methods proposed by Zhang et al.[19,20] and Chen et al.[21] are sensitive to serious noise.

In this article, one ACM based on multiple descriptors (MDACM) is presented. And the proposed method is capable of effectively dealing with the intensity inhomogeneity and serious noised image. Moreover, the proposed algorithm can complete segmentation and bias correction at the same time. In our method, local entropy is introduced to describe the intensity distribution combined with the means and the variance, which can yield more accuracy segmentation. Besides, the MDACM is more robust to noise because we adopt the entropy for the local gray statistic. Two level set functions are utilized to segment white matter, gray matter, cerebrospinal fluid, and background. Additionally, by introducing bias field factor, the MDACM can complete bias correction at the same time of segmentation.

The proposed segmentation model can be embedded into the visual module of brain surgery robots and help to obtain the accurate segmentation of brain tissue. The segmentation results can provide important information for the diagnosis and treatment of brain diseases. These preliminary processing can not only reduce the burden of doctors but also improve the success rate of operation.

The remaining parts are arranged as follows: "Background" section gives reviews of some typical ACM. "Proposed method" section introduces the new MDACM model. "Experimental results" section gives the results of brain MR image segmentation. The final section gives the conclusion.

Background

The LBF model

The LBF model takes full advantage of the local intensity information to achieve the segmentation for images with inhomogeneous intensity.[8,18] The LBF energy can be expressed as following

$$\begin{aligned} E^{\mathrm{LBF}}(\phi, f_1, f_2) &= \nu \int_{\Omega} \frac{1}{2}(|\nabla\phi| - 1)^2 \,\mathrm{d}x + \mu \int_{\Omega} \delta_{\varepsilon}(\phi)|\nabla\phi| \,\mathrm{d}x \\ &\quad + \lambda_1 \int \left[\int K(x-y)\Big(I(y) - f_1(x)\Big)^2 H_{\varepsilon}(\phi) \,\mathrm{d}y \,\mathrm{d}x \right. \\ &\quad + \lambda_2 \int \left[\int K(x-y)\Big(I(y) - f_2(x)\Big)^2 (1 - H_{\varepsilon}(\phi)) \,\mathrm{d}y \,\mathrm{d}x \right. \end{aligned} \tag{1}$$

where υ, μ, λ_1, and λ_2 are weighting non-negative constants and $K(x-y)$ is a window function.

As the LBF uses local means f_1 and f_2 as feature descriptor only, it could fail to deal with some images in accurate results. It is a two-phase segmentation model. It is sensitive to noise and cannot use for bias field estimation.

The LGDF model

In the study,[9] the local gray statistics are described with both means and variances, which enable LGDF with better robustness on the intensity inhomogeneity. In Bayesian framework, Wang et al. proposed the following energy functional

$$\begin{aligned} E^{\mathrm{LGDF}}(\phi,u_1,u_2,\sigma_1,\sigma_2) &= \nu\int_\Omega \frac{1}{2}(|\nabla\phi|-1)^2\,\mathrm{d}x + \mu\int_\Omega \delta_\varepsilon(\phi)|\nabla\phi|\,\mathrm{d}x \\ &- \int\left[\int K(x-y)p_{1,x}(I(y))H_\varepsilon(\phi(y))\,\mathrm{d}y\right]\mathrm{d}x \\ &- \int\left[\int K(x-y)p_{2,x}(I(y))(1-H_\varepsilon(\phi(y)))\,\mathrm{d}y\right]\mathrm{d}x \end{aligned} \tag{2}$$

where $p_{i,x}(I(y))$ is the intensity distribution function of the partition $\Omega_i \cap \boldsymbol{O}_x$.

Because the LGDF model utilizes two descriptors, both mean and variance, it is more robust to images with inhomogeneous intensity. But the segmentation accurate is not good enough for the images with complex brain tissue structure. And it is two-phase segmentation and no bias field estimation.

The local intensity clustering model

In the study,[14] an ACM based on local intensity clustering (LIC) is proposed. And a defined bias field is used to represent the intensity inhomogeneity. The LIC energy functional can be expressed as follows

$$\begin{aligned} E^{\mathrm{LIC}}(\phi,b,z_1,z_2) &= \nu\int_\Omega \frac{1}{2}(|\nabla\phi|-1)^2\,\mathrm{d}x + \mu\int_\Omega \delta_\varepsilon(\phi)|\nabla\phi|\,\mathrm{d}x \\ &+ \int\left[\int K(x-y)\Big(I(y)-b(x)z_1\Big)^2 H_\varepsilon(\phi(y))\,\mathrm{d}y\right]\mathrm{d}x \\ &+ \int\left[\int K(x-y)\Big(I(y)-b(x)z_2\Big)^2 (1-H_\varepsilon(\phi(y)))\,\mathrm{d}y\right]\mathrm{d}x \end{aligned} \tag{3}$$

where z_1 and z_2 are means and b is the bias factor.

The LIC can achieve segmentation as well as bias field correction. And it can realize multiphase segmentation and better results in accuracy, efficiency, and robustness. Nevertheless, it is not able to deal with the images at the presence of serious noise.

Proposed method

Local entropy

In Shannon's information theory,[22] a probabilistic system includes n events, and if the occurrence probability of an event i is p_i, then the information quantity of event i is defined as following

$$I = -\log_2 p_i \ (0 \le p_i \le 1) \tag{4}$$

And the information quantity of the whole probabilistic system with n events is defined as

$$H = -\sum_{i=1}^{n}\Big(p_i \log_2(p_i)\Big) \tag{5}$$

SHIOZAKI proposed to use the definition of SHANNON entropy to represent the image entropy.[23] The entropy of $M \times N$ image is defined as follows

$$H = -\sum_{i=1}^{M}\sum_{j=1}^{N} p_{ij}\log_2 p_i / \log_2(MN) \tag{6}$$

where p_i is the probability density of a given image. There is no generous definition for image intensity probability. Generally, there are two forms of definition, image gray histogram statistics and normalization of pixel value. The former is applicable to the threshold segmentation method and the latter is suitable for the ACM. The latter is chosen in this article defined as

$$p_{ij} = f(i,j) \Big/ \sum_{i=1}^{M}\sum_{j=1}^{N} f(i,j) \tag{7}$$

where $f(i,j)$ is the pixel value of one point with coordinate (i,j).

The different parts of images have different information. To describe the local image, we define the entropy of a continuous subarea Ω_x as

$$H(x,\Omega_x) = -\frac{1}{\log_2|\Omega_x|}\int_{\Omega_x} p(y,\Omega_x)(p(y,\Omega_x)-1)dy \tag{8}$$

where $p(y,\Omega_x)$ is the image intensity distribution probability.

The entropy can reflect the richness of image information. And it can be used as the measurement standard of the homogeneity of the partition. The partition is more homogeneous, and the entropy is higher.

In the proposed method, we take the local entropy together with mean and variance as the local image descriptors to obtain higher fitting degree for image intensity distribution. The value of local entropy is not sensitive to a single noise pixel because it is determined by several pixels in a continuous domain. And therefore the local entropy has a certain filtering effect. In addition, the normalization of intensity probability can also smooth the noise, which can guarantee the robustness to noise of our MDACM method,

especially for segmentation brain MR image with serious noises.

Image model

The proposed algorithm adopts the following common model to describe the images in the presence of inhomogeneous intensity

$$I = bJ + n \tag{9}$$

where I is the observed image, b is the inhomogeneous intensity component, J standards for the true image, and n is additive noise. The whole image domain is represented with Ω. The following part is the more detailed statement of J and b.[14,22]

Assumption 1: The inhomogeneous intensity component b changes slowly, so the value of b in the neighborhood of point x is approximately a constant, that is, $b(y) \approx b(x), y \in \boldsymbol{O}_x$.

Assumption 2: Image J includes N disjoint regions, that is, $\{\Omega_i\}_{i=1}^N$, $\Omega = \cup_{i=1}^N \Omega_i$, $\Omega_i \cap \Omega_j = \varnothing$, $i \neq j$. The intensity values of every distinct region are approximated as a constant denoted by $\{z_i\}_{i=1}^N$.

Therefore, we have the value of subneighborhood $\boldsymbol{O}_x \cap \Omega_i$ as

$$I(y) \approx b(x)z_i + n(y) \quad y \in \boldsymbol{O}_x \cap \Omega_i \tag{10}$$

MDACM fitting energy

We take the mean, variance, and entropy of image as descriptors to fit intensity distribution. The data fitting term of the model is defined in the Bayesian framework. So the fitting energy of every point can be written as

$$E_x = H_x \bullet \sum_{i=1}^{N} \lambda_i \int_{\Omega_i \cap \Omega_x} -\log \; p_{i,x}\Big(I(y)\Big)dy \tag{11}$$

where λ_i is positive constant, H_x is the entropy of the neighborhood of point x, and $p_{i,x}(I(y))$ represents the intensity probability of subneighborhood. In this article, the probability is assumed to be Gaussian distribution, that is

$$p_{i,x}\left(I(y)\right) = \frac{1}{\sqrt{2}\pi\sigma_i(x)} \exp\left(-\frac{\Big(I(y) - b(x)z_i\Big)^2}{2\sigma_i(x)^2}\right) \tag{12}$$

where z_i is the local means and $\sigma_i(x)$ is the local variances. Then we obtain

$$E_x = H_x \bullet \sum_{i=1}^{N} \lambda_i \int_{\Omega_i \cap \Omega_x} \left(\log \sigma_i(x) + \frac{(I(y) - b(x)z_i)^2}{2\sigma_i^2(x)}\right) dy \tag{13}$$

Then we introduce a non-negative window function $k(u)$, also called kernel function, to limit the neighborhood field. The window function $k(u)$ selected here is defined as

$$k(u)\begin{cases} a, & |u| \leq \rho \\ 0, & |i| > \rho \end{cases} \tag{14}$$

where a is a positive constant and $\int k(u) = 1$. With $k(u)$, the local fitting energy E_x of one point x can be rewritten as

$$E_x = H_x \bullet \sum_{i=1}^{N} \lambda_i \bullet \int_{\Omega_i} k(x-y) \bullet \left(\log \sigma_i(x) + \frac{(I(y) - b(x)z_i)^2}{2\sigma_i^2(x)}\right) \mathrm{dy} \tag{15}$$

The above E_x is minimized when the zero level set coincides with the edge of the object and the fitting values b, z_i, and σ_i are optimal. The E_x defined in expression (15) is only for one point x, so the minimization of E_x can only obtain part of boundary. By integrating the E_x in the whole image domain Ω, we can get the global fitting energy of the image E_d, then find the entire object boundary by minimizing E_d. The global fitting energy E_d is rewritten as

$$E_d = \int_{\Omega} H_x \bullet \sum_{i=1}^{N} \lambda_i \bullet \int_{\Omega_i} k(x-y) \bullet \left(\log \sigma_i(x) + \frac{(I(y) - b(x)z_i)^2}{2\sigma_i^2(x)}\right) \mathrm{dydx} \tag{16}$$

where the local entropy H_x quantifying the intensity changes in neighborhood is introduced as the weight of one point fitting energy. When the point x is a noise pixel, the value of local entropy is very small so that it has little impact on E_d. In contrast, the value is big to accelerate the contour evolution to the object boundary.

MDACM

It is difficult to get the solution of the minimization of E_d in equation (16). So we convert the king formula to a level set form. In this form, we can use several level set functions to represent those disjoint regions and then use the calculative variational method to minimize the energy functional.

In traditional two-phase segmentation, only one level set function is enough to divide the image into foreground and background. In multi-phase segmentation $N > 2$, we will compose N membership functions M_i to stand for different region with more than two level set functions. The brain MR image has four parts, and it is necessary to complete the four-phase segmentation. We introduce ϕ_1 and ϕ_2 to define four membership functions M_i as follows

$$\begin{cases} M_1(\phi_1, \phi_2) = H(\phi_1)H(\phi_2) \\ M_2(\phi_1, \phi_2) = H(\phi_1)(1 - H(\phi_2)) \\ M_3(\phi_1, \phi_2) = (1 - H(\phi_1))H(\phi_2) \\ M_4\phi_1, \phi_2) = (1 - H(\phi_1))(-H(\phi_2)) \end{cases} \tag{17}$$

where ϕ_1 and ϕ_2 are level set functions. And the Heaviside function is introduced as

$$H_\varepsilon(z) = \frac{1}{2}\left[1 + \frac{2}{\pi}\arctan\left(\frac{z}{\varepsilon}\right)\right] \tag{18}$$

The differential of H is denoted as δ, which is computed by

$$\delta_\varepsilon(z) = \frac{1}{\pi}\cdot\frac{\varepsilon}{\varepsilon^2 + z^2} \tag{19}$$

So the final data fitting term of the four-phase model for brain MR image is rewritten in the following form

$$\begin{aligned} E_d(\Phi, b, Z, \Theta) = \int_\Omega H_x \bullet \left(\sum_{i=1}^{4}\lambda_i \bullet \int_{\Omega_i} k(x-y)\bullet \right. \\ \left. \left(\log\sigma_i(x) + \frac{(I(y) - b(x)z_i)^2}{2\sigma_i^2(x)}\right) M_i dy\right) dx \end{aligned} \tag{20}$$

For convenience, where we represent the constants z_1,z_2,z_3,z_4 with a vector $Z = (z_1, z_2, z_3, z_4)$, the vector $\Theta = (\sigma_1, \sigma_2, \sigma_3, \sigma_4)$ for variances σ_1,σ_2, σ_3,σ_4, and two level set functions ϕ_1 and ϕ_2 with a vector $\Phi = (\phi_1, \phi_2)$.

The energy E_d is introduced as the data part in the proposed MDACM method. The total energy of the MDACM model is defined by

$$E(\Phi, b, Z, \Theta) = E_d(\Phi, b, Z, \Theta) + \mu R(\Phi) + \upsilon L(\Phi) \tag{21}$$

where μ and υ are positive coefficients. The second term is the regularizing term, which can ensure stable evolution of ϕ. The deviation of ϕ from the signed distance function is defined as following

$$R(\Phi) = \int_\Omega \frac{1}{2}(|\nabla\phi_1| - 1)^2\,\mathrm{d}x + \int_\Omega \frac{1}{2}(|\nabla\phi_2| - 1)^2\,\mathrm{d}x \tag{22}$$

The third term is the length regularization term. And whose definition formula is

$$L(\Phi) = \int_\Omega \delta_\varepsilon(\phi_1)|\nabla\phi_1|\,\mathrm{d}x + \int_\Omega \delta_\varepsilon(\phi_2)|\nabla\phi_2|\,\mathrm{d}x \tag{23}$$

To get the correct boundary, we minimize the energy functional.

Energy minimization

The gradient descent method is used to complete the minimization of the total energy formula (21) for image segmentation. Image segmentation is achieved by iterative process, taking one variable in turn to iterate.

Each variable and the level set evolution formula are given as follows.

By fixing the variables Φ, b, Θ and minimizing E relate to $E(\Phi, b, Z, \Theta)$, the expression of the mean vector $Z = (z_1, z_2, z_3, z_4)$ is given as

$$z_i = \frac{\int\left(k * \frac{b}{\sigma_i^2}\right) I(y) M_i dy}{\int\left(k * \frac{b}{\sigma_i^2}\right) M_i dy}, \quad i = 1, 2, 3, 4 \tag{24}$$

By fixing the variables Φ, b, Z and minimizing $E(\Phi, b, Z, \Theta)$ relate to Θ, the expression of the variance vector $\Theta = (\sigma_1, \sigma_2, \sigma_3, \sigma_4)$ is given as

$$\sigma_i^2(x) = \frac{\int k(x-y)(I(y) - b(x)z_i)^2 M_i dy}{\int k(x-y) M_i dy} \tag{25}$$

By fixing the variables Φ, Θ, Z and minimizing $E(\Phi, b, Z, \Theta)$ relate to b, the expression of the bias field b is given as

$$b(x) = \frac{\sum_{i=1}^{4}\int_\Omega k(x-y)\frac{z_i}{\sigma_i^2} I(y) M_i dy}{\sum_{i=1}^{4}\int_\Omega k(x-y)\frac{z_i}{\sigma_i^2} M_i dy} \tag{26}$$

Keeping b, Z, and Θ fixed and minimizing $E(\Phi, b, Z, \Theta)$ relate to Φ, we get the level set evolution formula as follows

$$\begin{aligned} \frac{\partial\phi_1}{\partial t} &= \delta_\varepsilon(\phi_1)(\lambda_3 e_3 - \lambda_1 e_1) H(\phi_2) \\ &\quad + \delta_\varepsilon(\phi_1)(\lambda_4 e_4 - \lambda_2 e_2)(1 - H(\phi_2) \\ &\quad + \mu\left[\nabla^2(\phi_1) - div\left(\frac{\nabla(\phi_1)}{|\nabla(\phi_1)|}\right)\right] \\ &\quad + \upsilon\delta_\varepsilon(\phi_1) div\left(\frac{\nabla(\phi_1)}{|\nabla(\phi_1)|}\right) \end{aligned} \tag{27}$$

$$\begin{aligned} \frac{\partial\phi_2}{\partial t} &= \delta_\varepsilon(\phi_2)(\lambda_2 e_2 - \lambda_1 e_1) H(\phi_1) \\ &\quad + \delta_\varepsilon(\phi_2)(\lambda_4 e_4 - \lambda_3 e_3)(1 - H(\phi_1)) \\ &\quad + \mu\left[\nabla^2(\phi_2) - div\left(\frac{\nabla(\phi_2)}{|\nabla(\phi_2)|}\right)\right] \\ &\quad + \upsilon\delta_\varepsilon(\phi_2) div\left(\frac{\nabla(\phi_2)}{|\nabla(\phi_2)|}\right) \end{aligned} \tag{28}$$

where e_i is induced for notational simplicity, given as follows

$$e_i = \int H_x k(x-y)\left(\log\sigma_i(x) + \frac{(I(y) - b(x)z_i)^2}{2\sigma_i(x)}\right) dy \tag{29}$$

Implementation

The implementation of our algorithm includes the following seven steps:

Step 1: Compute the local entropy H_x.
Step 2: Initialize the level set functions ϕ_1 and ϕ_2 bias factor b.
Step 3: Calculate the means z_1, z_2, z_3, and z_4.
Step 4: Calculate the variances σ_1^2, σ_2^2, σ_3^2, and σ_4^2.
Step 5: Update the level set functions ϕ_1 and ϕ_2.
Step 6: Update the bias factor b.
Step 7: Check whether meet the convergence criteria. If not, rerun Step3.

Experimental results

To evaluate the performance of the MDACM, we apply it to some brain MR image. The experiments are implemented in Matlab 2013 in PC with Inter CPU 3.20 and 4 GB RAM and Windows 7 operating system. In this section, the parameters are as follows:$\lambda_1 = \lambda_2 = \lambda_3 = \lambda_4 = 1$, $\mu = 1.0$, ρ=21, $r = 4.5$, $\upsilon = 0.05 \times 255 \times 255$, time step $\Delta t = 0.1$. Our method is compared with the multiphase LBF model and the LIC model to validate its effectiveness.

The validity of MDACM

The first experiment is designed to demonstrate the validity of the MDACM model. We apply it to segment brain MR image and correct the bias field.

The experiment results are shown in Figure 1. Figure 1(a), (b), (c), and (d), respectively, shows the original images, segmentation result images, bias field images, and images after correction. It is obvious that the intensity distribution of the same tissue is more homogeneous in the images after correction than in the original images. Figure 1(e) displays the histograms of original images. Figure 1(f) displays the histograms of the images after correction. It can be seen that the histogram of original image has no well-separated peaks because of the inhomogeneous intensity. However, the histogram shown in Figure 1(f) has three well-separated peaks. The inhomogenous intensity in the images has been obviously improved.

The experiment results in this subsection show that the MDACM has the ability of segmenting the brain MR image with inhomogeneous intensity as well as correcting bias field.

Comparison with multiphase LBF model and LIC model

The second experiment is designed to show the comparison of the segmentation accuracy. The three models of MDACM, multiphase LBF, and LIC are employed in segmenting the brain MR image as shown in Figure 2.

The original images with intensity inhomogeneity are shown in Figure 2(a). The results of the multiphase LBF, the LIC, and the MDACM are shown in Figure 2(b) to (d). In Figure 2(b) to 2(d), these three models segment the brain

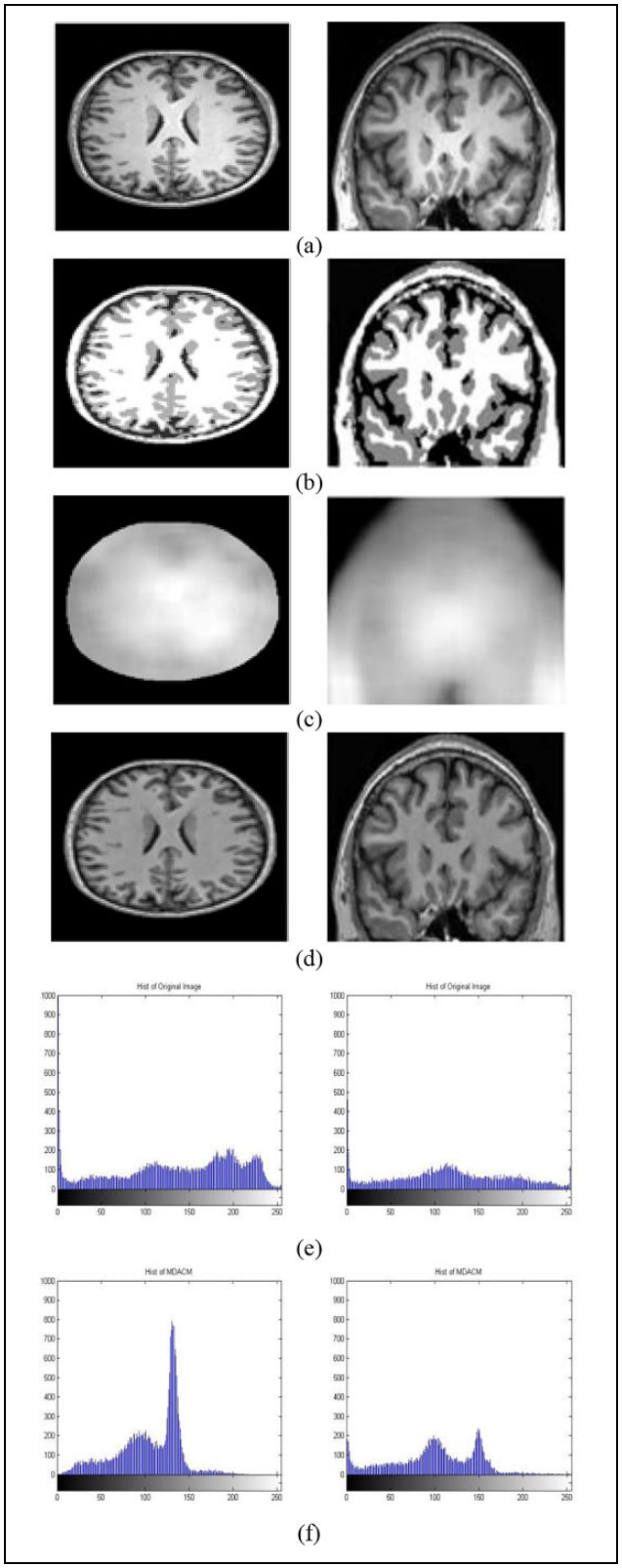

Figure 1. Applications of MDACM to brain MR image with inhomogeneous intensity. (a) Original images; (b) segmentation results; (c) bias fields; (d) bias-corrected images; (e) histograms of the original images; (f) histograms of the bias corrected images. MR: magnetic resonance.

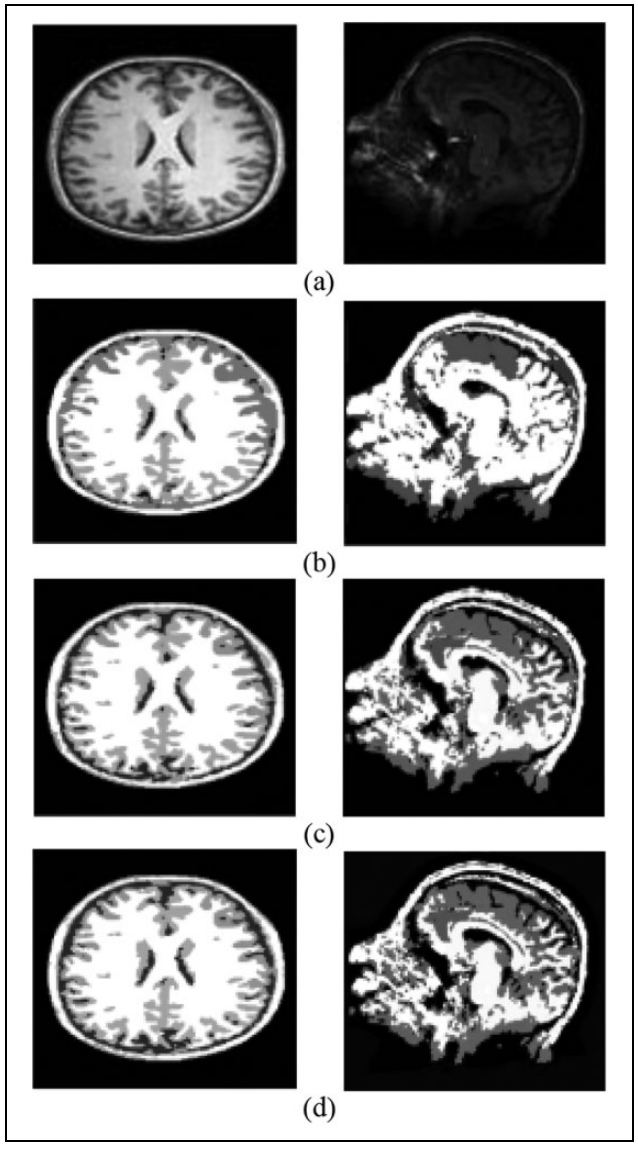

Figure 2. Comparison of the MDACM with the multiphase LBF and the LIC models for brain MR image. (a) Original images; (b) results of the multiphase LBF; (c) results of the LIC; (d) results of the MDACM. MR: magnetic resonance; LBF: local binary fitting; LIC: local intensity clustering.

MR image with different results. As shown in Figure 2(b), there are lots of errors in sedimentation of cerebrospinal fluid as gray matter. Compared with the multiphase LBF model, the LIC has better segmentation results as shown in Figure 2(c). However, there are still some false segmentation regions in brain tissue. In contrast, the proposed method has the best segmentation results that are most similar to the true segmentation.

In order to give a quantitative comparison of our MDACM model with the other two models, we select the dice similarity coefficient (DSC), the false negative ratio (FNR), the false positive ratio (FPR), and the ratio of segmentation error (RSE) to descript the segmentation accuracy.[24] Figure 3 is the histogram of the DSC value.

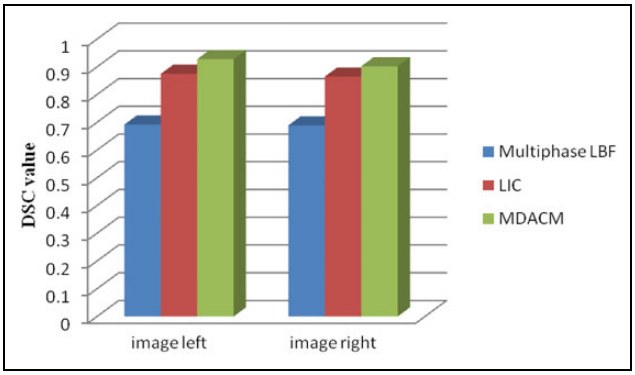

Figure 3. Accuracy comparison of the three models for brain MR image. MR: magnetic resonance.

Table 1. FNR, FPR, and RSE values.

Model	FNR	FPR	RSE
Multiphase LBF	0.1052	0.0608	0.0425
LIC	0.0823	0.0411	0.0240
MDACM	0.0307	0.0152	0.0081

FNR: false negative ratio; FPR: false positive ratio; RSE: ratio of segmentation error; LBF: local binary fitting; LIC: local intensity clustering.

And Table 1 lists the data statistics for the other three indexes. The ideal segmentation results should be DSC→1, FPR→0, FNR→0, RSE→0.

As can be seen from Figure 3, for the left image, the DSC value of the proposed algorithm MDACM is close to 0.9, the LIC has a DSC value of 0.85, while the DSC value of the multiphase LBF is 0.78. And for the right image, the DSC value of the MDACM is 0.88, the LIC has a DSC value of 0.83, while the DSC value of the multiphase LBF is 0.67. Obviously, the proposed algorithm has the highest DSC value and the best segmentation effect.

In Table 1, the value of each index is the average number of two images. And the values of the MDACM are the lowest, with the FNR 0.0307, the FPR 0.0152, and the RSE 0.0081.The values of the multiphase LBF are the highest, with the FNR 0.0307, the FPR 0.0152, and the RSE 0.0081. And the values of the LIC are between the above two methods. The data show that the proposed MDACM algorithm has the best segmentation effect.

The MDACM is obviously superior to the multiphase LBF method. On the one hand, the two descriptors, such as variance and local entropy, are added, so the intensity description is more accurate. On the other hand, the algorithm realizes the bias field correction, so the effect of intensity inhomogeneity on segmentation is weakened. The LIC algorithm takes into account the bias field compared with the multiphase LBF, so the performance is better than the multiphase LBF. While compared with the proposed MDACM, the LIC lacks two descriptors of variance and local entropy, so the accuracy is lower than the MDACM.

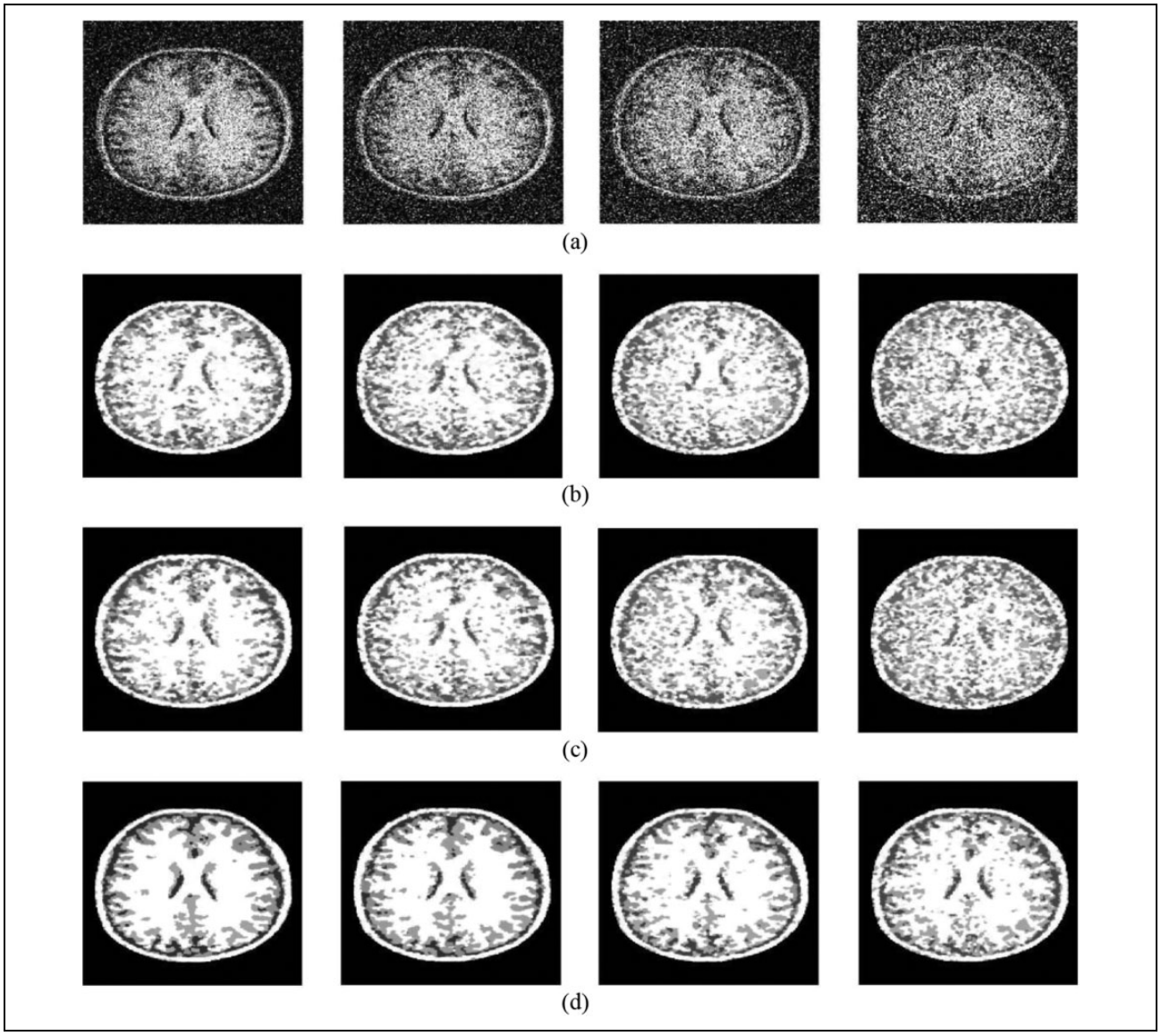

Figure 4. Segmentation results for the images with different Gaussian white noise. (a) Noisy brain MR image; (b) results of multiphase LBF; (c) results of LIC; (d) results of the proposed method. MR: magnetic resonance; LBF: local binary fitting; LIC: local intensity clustering.

Robustness to noise

The proposed method is robust, which is validated in the third experiment. The segmentation results of noisy images for the multiphase LBF, the LIC, and the MDACM are shown in Figure 4. The same images corrupted with Gaussian white noise with different standard deviations are shown in Figure 4(a). The standard deviations of Gaussian noise are 0.1, 0.15, 0.2, and 0.5 from left to right. Figure 4(b) and (c) shows the segmentation images of the multiphase LBF and the LIC. Figure 4(d) shows the segmentation of the MDACM. It is obvious that the segmentation results of the MDACM model are better than the other two methods.

To give a quantitative comparison, we also select the DSC, the FNR, the FPR, and the RSE to descript the segmentation accuracy. The corresponding DSC values of three models are shown in Figure 5. The values of FNR, FPR, and RSE are listed in Table 2.

As can be seen from Figure 5, in the case of the same noise, the DSC value of the proposed MDACM is the highest and the DSC value of the multiphase LBF is the lowest. For example, when the standard deviation of Gaussian noise is 0.1, the DSC of the MDACM is close to 0.8, the DSC value of the LIC is 0.61, and the DSC value of the multiphase LBF is only 0.53. The DSC value of the MDACM is nearly 60% higher than that of the multiphase LBF. And when the standard deviation of Gaussian noise is 0.5, the DSC of the MDACM is 0.63, the DSC value of the LIC is 0.37, and the DSC value of the multiphase LBF is only 0.32. The DSC value of the MDACM is nearly 100% higher than that of the multiphase LBF. It is worth noting

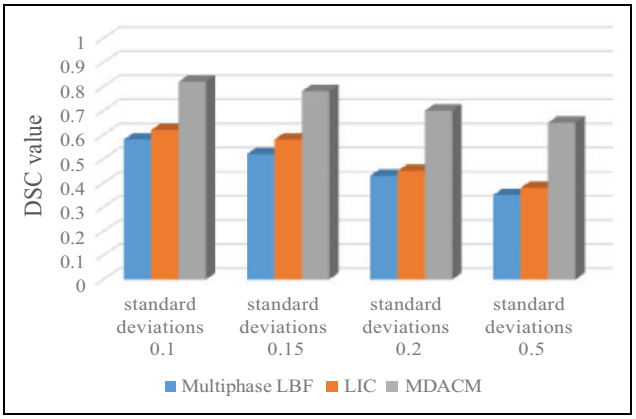

Figure 5. Robustness to noise comparison of the three models.

Table 2. FNR, FPR, and RSE values.

Model	FNR	FPR	RSE
Multiphase LBF	0.5125	0.4768	0.3532
LIC	0.4012	0.3798	0.2117
MDACM	0.1205	0.0801	0.0627

FNR: false negative ratio; FPR: false positive ratio; RSE: ratio of segmentation error; LBF: local binary fitting; LIC: local intensity clustering.

that with the increase of noise level, the DSC values of various methods are decreased, and the decrease value of the MDACM is the least, which shows that the proposed MDACM has the best performance of robustness to noise.

As can be seen from Table 2, MDACM has the lowest FNR value of 0.1205, the lowest FPR value of 0.0801, and the lowest RSE value of 0.0627. While the multiphase LBF has the highest FNR value of 0.5125, the highest FPR value is 0.4768, the highest RSE value is 0.3532, and all above values are close to 5 times of those of MDACM.

The data in Figure 5 and Table 2 show that the proposed MDACM method has better robustness to noise than the multiphase LBF model and the LIC model. The main reason is that the algorithm introduces the local entropy as the descriptor on the basis of mean and variance, and the local entropy has the effect of smoothing noise. So the anti-noise performance of the algorithm is improved.

Conclusion

In this article, one multiphase ACM segmentation method named MDACM for brain MR image with inhomogeneous intensity and serious noise is proposed, which can be embedded into the visual module of brain surgery robots. Our model utilizes multiple descriptors, the mean, the variance, and the local entropy to guarantee the exhaustive expression of the local intensity distribution. The local entropy is successfully introduced to obtain desirable performance in the aspect of robustness to noise. The proposed method can complete segmentation and bias correction for brain MR image. Experimental results show our method meets all the four conditions of accurate segmentation of brain tissue: the full description of gray value distribution, robust to serious noise, multiphase segmentation, and bias field estimation. Comparisons with the LIC and the multiphase LBF models, experimental results demonstrate that the MDACM has better performance on the aspects of accuracy and robustness to serious noise. While achieving better accuracy, there are still some works to be improved. In the future, more efforts will be made to further improve the robustness to noise and real-time performance to adapt to the requirements of high precision and real-time of brain surgery robots. In addition, the MDACM model will be embedded into brain surgery robot for clinical tests to further improve the accuracy and applicability of the algorithm according to the doctor's advises. It is believed that this will improve the localization of brain lesions and the success rate of surgery.

Declaration of conflicting interests

The authors declared no potential conflicts of interest with respect to research, authorship, and/or publication of this article.

Funding

The author(s) disclosed receipt of the following financial support for the research, authorship, and/or publication of this article: This work is supported by the National Science Foundation of China (61503274 and 61603080), and Fundamental Research Funds for the Central Universities (N16260004).

References

1. Faria C, Erlhagen W, Manuel R, et al. Review of robotic technology for stereotactic neurosurgery. *IEEE Rev Biomed Eng* 2015; 1(8): 125–137.
2. Maddahi Y, Gan LS, Zareinia K, et al. Quantifying workspace and forces of surgical dissection robot-assisted neurosurgery (Report). *Int J Med Robot Comp* 2016; 12(3): 528–538.
3. Miura S, Kobayashi Y, Kawamura K, et al. Brain activation in parietal area during manipulation with a surgical robot simulator. *Int J Med Robot Comp* 2015; 10(6): 783–790.
4. Chen GD, Jia PF, and Wang RJ. Space registration and practice of a brain surgery robot based on optical localization. *Chin J Sci Instrum* 2007; 28(3): 499–503.
5. Yoshizawa A, Jun O, Yamakawa MG, et al. Robot surgery based on the physical properties of the brain-physical brain model for planning and navigation of a surgical robot. In: *IEEE international conference on robotics and automation*, 2005, pp. 904–911.
6. Kass M, Witkin A, and Terzopoulos D. Snakes: active contour models. *Int J Comput Vision* 1988; 1: 321–331.
7. Vese L and Chan T. A multiphase level set framework for image segmentation using the Mumford and Shah model. *Int J Comput Vision* 2002; 50(3): 271–293.
8. Li C, Kao C, Gore J, et al. Implicit active contours driven by local binary fitting energy. In: *IEEE conference on computer vision and pattern recognition*, 2007, pp. 1–7.

9. Wang L, He L, Mishra A, et al. Active contours driven by local Gaussian distribution fitting energy. *Signal Proc* 2009; 89(12): 2435–2447.
10. Zhang K, Song H, and Zhang L. Active contours driven by local image fitting energy. *Pattern Recogn* 2010; 43: 1199–1206.
11. Liu S and Peng Y. A local region-based Chan-Vese model for image segmentation. *Pattern Recogn* 2012; 45(7): 2769–2779.
12. Dong F, Chen Z, and Wang J. A new level set method for inhomogeneous image segmentation. *Image Vision Comput* 2013; 31(10): 809–831.
13. Akram F, Kim JH, Lim H, et al. Segmentation of intensity inhomogeneous brain MR image using active contours. *Comput Math Method M* 2014; 22(3): 1–14.
14. Li CM, Huang R, Ding Z, et al. A level set method for image segmentation in the presence of intensity inhomogeneities with application to MRI. *IEEE Trans Image Proc* 2011; 20(7): 2007–2016.
15. Li CM, Gore JC, and Davatzikos C. Multiplicative intrinsic component optimization (MICO) for MRI bias field estimation and tissue segmentation. *Magn Reson Imaging* 2014; 32(7): 913–923.
16. Gharge S and Bhatia M. Statistical analysis of brain MRI Image segmentation for the level set method. *Int J Appl Innov Eng Manage (IJAIEM)* 2013; 2(6): 491–496.
17. Konduri SS and Thirupathaiah A. A level set image articulations in presence of disagree-ement with MRI scanning. *Int J Res Comput Commun Technol* 2014; 3(1): 1–4.
18. Zhang K, Liu Q, Song H, et al. A variational approach to simultaneous image segmentation and bias correction. *IEEE Trans Cybern* 2015; 45(5): 1426–1437.
19. Zhang KH, Zhang L, and Zhang S. A variational multiphase level set approach to simultaneo-us segmentation and bias correction. In: *International conference on image processing*, Hong Kong, China, 26–29 September 2010. IEEE.
20. Zhang KH, Zhang L, Lam KM, et al. A level set approach to image segmentation with intensity inhomogeneity. *IEEE Trans Cybern* 2016; 46(2): 546–557.
21. Chen Y, Wang Z, Jevon B, et al. An automatical segmentation method for brain MR images. *Adv Sci Technol Letters* 2016; 123(1): 171–177.
22. Shannon CE. A mathematical theory of communication. *Bell Syst Tech J* 1948; 27(2): 379–423.
23. Shiozaki A. Edge extraction using entropy operator. *Comput Vision Graph Image Pro* 1986; 36(4): 1–9.
24. Wang L, Li CM, Sun QS, et al. Active contours driven by local and global intensity fitting energy with application to brain MR image segmentation. *Comput Med Imag Grap* 2009; 33(7): 520–231.